Phase diagram and thermodynamic properties of H_2

S. M. Osman,* I. Ali, and R. N. Singh
Department of Physics, College of Science P O Box 36, Al-Khod 123 Sultan Qaboos University, Sultanate of Oman
(Received 9 June 2012; published 18 January 2013)

A statistical mechanical-based theory is used to develop the equation of state for the molecular fluid of H_2. We incorporate in this equation the long-range correlations through the double Yukawa potential, dimerization of the H_2 molecule by treating the fluid as a hard convex body fluid, and first-order quantum correction which is important at low temperatures. We use this to calculate the liquid-vapor equilibrium of H_2, including the temperature and pressure dependence of compressibility factor, entropy, specific heat, compressibility, and sound velocity.

DOI: 10.1103/PhysRevE.87.012122 PACS number(s): 05.70.−a, 64.10.+h, 67.10.Fj, 64.70.F−

I. INTRODUCTION

The temperature- and pressure-dependent properties of fluid molecular hydrogen (H_2) are of considerable significance. H_2 is increasingly considered in fuel cell technology *vis a vis* it is one of the most abundant species of the interstellar space. It is widely perceived as an environmentally clean and renewable energy source. Studies [1,2] indicate that H_2 becomes metallic at sufficiently high pressures, between 100 and 600 GPa. A detailed investigation of the equation of state (EOS) and the thermodynamics properties is essential to understand the behavior of H_2.

In this work, we have used statistical mechanical perturbation theory to set up the EOS of H_2. The short-range repulsive potential is treated here as the unperturbed hard sphere reference system. On the other hand, the long-range attractive correlations are included via the double Yukawa potential as a first-order perturbation correction. The dimerization of the H_2 molecule is treated as a hard convex body fluid (HCB) for which an EOS can be derived based on scaled particle theory [3,4]. The quantum correction is included through Wigner-Kirkwood expansion [5,6]. Taking into account the various contributions, we have been able to suggest an improved version of EOS to study the compressibility factor Z, excess entropy, specific heat, isothermal and adiabatic compressibilities, and speed of sound of fluid H_2 as functions of temperature and pressure.

This work is divided as follows: Useful formulations for the EOS are formulated in Sec. II. The liquid-vapor equilibrium curves for H_2 are given in Sec. III. Section IV provides the computed results of the compression factor and isochoric density as functions of temperature. We include in Sec. V thermophysical properties, where entropy, specific heat, compressibility, and thermal expansion are presented as functions of T and p. The impact of T and p on the velocity of sound is presented in Sec. VI, followed by a summary and conclusion in Sec. VII.

II. EQUATION OF STATE FOR H_2 FLUID

The complexities of the intermolecular interactions and the dimerization of the H_2 molecule pose a considerable hindrance to obtaining theoretical expressions for the EOS. We utilize here a realistic EOS developed for nonspherical hard body fluids:

$$\frac{\beta P}{\rho} = \rho \frac{\partial}{\partial \rho} \frac{F}{NkT}. \tag{1}$$

$\beta = (kT)^{-1}$, P stands for pressure, ρ is the density, k is Boltzmann constant, and F is the Helmholtz free energy. Central to the theoretical evaluation of F is the inclusion of H_2 dimerization. The dimerization has been treated here in the form of a HCB for which a realistic EOS for hard nonspherical molecules exists [3]. The basic idea is to modify the free energy of a hard sphere fluid F_{hs} with a geometrical shape factor a (the nonsphericity parameter) coming from the scaling theory [4].

An important limitation of the HCB EOS is that it does not include energetic effects arising due to long-range correlations and the quantum corrections for small-mass particles, particularly at low temperatures. The long-range attractive interactions among the constituent species has been included here via the double Yukawa (DY) potential, which acts as a perturbation on the reference systems of hard spheres. The advantage of using the DY potential is that it allows the variational integral equations of the energies to be derived analytically in terms of the Laplace transform of the radial distribution function. The quantum correction is included via the first-order correction in the Wigner-Kirkwood expansion [5,6].

Including these contributions, the Helmholtz free energy that results will consist of (i) the ideal term ($F_{\rm id}$), (ii) modified hard sphere energy for molecular fluids ($F_{\rm HCB}$), (iii) the first-order contribution due to attractive forces ($F_{\rm t}$), and (iv) the quantum energy correction ($F_{\rm Q}$). The total Helmholtz free energy per molecule for H_2 fluid can then be expressed as

$$F = F_{\rm id} + F_{\rm HCB} + F_{\rm t} + F_{\rm Q}, \tag{2}$$

with

$$\beta F_{\rm id} = \frac{3}{2} \ln \left(\frac{h^2 N_A}{2\pi M_{\rm H_2} kT} \right) + \ln \rho - 1, \tag{3}$$

$$F_{\rm HCB} = a F_{\rm SS}, \tag{4}$$

$$\beta F_{\rm t} = \frac{\beta \rho}{2} \int_{\sigma}^{\infty} u(r) g(r) 4\pi r^2 \overline{V} dr, \tag{5}$$

$$\beta F_{\rm Q} = \frac{\beta^2 \hbar^2 N_A \rho}{24\pi^2 M_{\rm H_2}} \int_{\sigma}^{\infty} \nabla^2 u(r) g(r) 4\pi r^2 \overline{V} dr. \tag{6}$$

*Corresponding author: osm@squ.edu.om

Here, $M_{H_2} = 2.015\,9$ g/mol is the molecular weight. Since the H_2 molecule is slightly nonspherical, a suitable nonsphericity parameter a and effective volume $\overline{V}$ can be introduced to account for the dimerization effect and improve the performance of the equation of state. The scaling parameters a and $\overline{V}$ appear in Eqs. (4)–(6), (21), (23), and (24) and are linked via the HCB scaling theory [3,4] as

$$\overline{V} = 1 + \left(3L - \frac{L^3}{2} - 3H\theta\right). \tag{7}$$

$\overline{V}$ is the volume factor for the average molecular volume. L, H, and θ stand for

$$L = \frac{l}{d}; \quad H = \left(1 - \frac{L^2}{4}\right)^2; \quad \theta = \sin^{-1}\left(\frac{L}{2}\right). \tag{8}$$

l is the center-to-center distance of the molecule (the length of the covalent bond), and d is the radius of the hydrogen atom. There exist several measurements of bond lengths and atomic radii of atomic molecules. The accuracy of the measurements depends on the method of calculation [7–9]. In the present work, we use the most accurate reported values of $l = 0.7461$ Å and $d = 1.2$ Å [10,11], which give satisfactory triple point parameters of liquid H_2. The nonsphericity parameter is defined as

$$a = \frac{1}{3\pi}\frac{V'_{\rm ef}V''_{\rm ef}}{V_{\rm ef}}, \tag{9}$$

where $V_{\rm ef} = \pi d^3\overline{V}/6$, and the symbols $'$ and $''$ are the first and second derivatives of the effective molecular volume $V_{\rm ef}$ with respect to d.

The usual soft sphere energy which is modified in Eq. (4) through the nonsphericity parameter a incorporated through the scaling theory [12,13], i.e.,

$$\begin{aligned}\beta F_{\rm SS} &= (a_1 + 3a_2 - 1)\ln(1-\eta) \\ &\quad + \frac{(6 + 2a_1 + 6a_2)\eta - (3 + 3a_1 + 9a_2)\eta^2 + 2a_2\eta^3}{2(1-\eta)^2} \\ &\quad - \frac{\eta}{2}[1 + 2\eta + \eta^3],\end{aligned} \tag{10}$$

with $\eta = \pi\rho\sigma^3/6$ (packing fraction, σ is the hard sphere diameter). The first two terms of Eq. (10) are the usual hard sphere excess free energy given by Baus and Colot [12] with $a_1 = a_2 = \frac{2}{3}$. The last term is the softening term given by Ross [13].

Central to the computation of the term $F_{\rm t}$ in Eq. (5) is the pairwise potential $u(r)$, which is assumed to consist of soft repulsion $u^{\rm ss}(r)$ (normally the soft sphere potential) and a long-range attraction $u^{\rm t}(r)$,

$$u(r) = u^{\rm ss}(r) + u^{\rm t}(r). \tag{11}$$

$u^{\rm ss}$ is treated as the unperturbed reference system of $1/r^{12}$ potential. Ross [13] performed computer simulation on fluids interacting via repulsive $1/r^{12}$ potential and obtained a correction term to the free energy of hard-sphere fluids. This softening term appears in Eq. (10). The second term of Eq. (11), $u^{\rm t}$, acts as a perturbation. The long-range attractive forces are included through the DY potential ($u^{\rm t} \equiv u^{\rm DY}$),

$$\begin{aligned}u^{\rm DY}(r) = E\epsilon_0\frac{\sigma_0}{r}\Bigg\{&\exp\left[-\lambda_1\left(\frac{r}{\sigma_0} - 1\right)\right] \\ &- \exp\left[-\lambda_2\left(\frac{r}{\sigma_0} - 1\right)\right]\Bigg\},\end{aligned} \tag{12}$$

where ϵ_0 is the potential depth, and σ_0 is the value at which $u^{\rm DY}(r) = 0$. E, λ_1, and λ_2 are the fitting potential parameters. The advantage of using the DY potential is that the relevant Helmholtz free energy can be found analytically, therefore providing an analytical expression for the EOS. We have used the Silvera-Goldman [14] potential for H_2 to obtain the DY parameters. The exponential-6 potential is found to be satisfactory over a wide range of temperatures and pressures. The resulting values for the DY potential are

$$\begin{aligned}&\sigma_0 = 3.013\ \text{Å}; \quad \frac{\epsilon_0}{k} = 31.757\ \text{K}; \quad E = 3.5116; \\ &\lambda_1 = 9.1341; \quad \lambda_2 = 3.6153.\end{aligned} \tag{13}$$

The optimized hard sphere diameter σ of the repulsive soft sphere potential is obtained by choosing σ to have temperature dependence, via the well known Gibbs-Bogolubov [15,16] prescription requiring that $F \leqslant F_{\rm SS} + F_{\rm t} + F_{\rm Q}$, namely,

$$\left(\frac{\partial F}{\partial \sigma}\right)_{\rho,T} = 0. \tag{14}$$

σ is the basic ingredient for the computation of the radial distribution function $g(r)$; hence, Eq. (14) provides a suitable link between structure and the pairwise interactions. For the perturbation free energy we used the most improved expressions for $g(r)$ due to Henderson *et al.* [17,18]. It is based on three ingredients: (i) the analytical solution of the OZ equation within mean spherical approximation of the direct correlation function $C(r)$, which is considered more accurate than the Percus-Yevick (PY) approximation; (ii) the inverse temperature expansion of $g(r)$ up to the fifth term; and (iii) satisfying the thermodynamic consistency conditions between the energy and compressibility equations of state, leading to analytical expressions to the five expansion coefficients of $g(r)$. The resulting expression of $g(r)$ is in excellent agreement with Monte Carlo simulation results as reported in Ref. [19].

Substituting $u(r)$ from Eq. (12), the integrations of Eqs. (5) and (6) can be performed analytically, yielding

$$\beta F_{\rm t} = \frac{\overline{V}E}{2\sigma^*}[e^{\lambda_1}G(\overline{\lambda}_1) - e^{\lambda_2}G(\overline{\lambda}_2)], \tag{15}$$

$$\beta F_{\rm Q} = \frac{A_Q\overline{V}E}{24\sigma^*}\left(\frac{\epsilon_0}{kT}\right)\left[\lambda_1^2 e^{\lambda_1}G(\overline{\lambda}_1) - \lambda_2^2 e^{\lambda_2}G(\overline{\lambda}_2)\right], \tag{16}$$

where $G(\lambda_i)$ $(i = 1, 2)$ is related to the Laplace transform of $rg(r)$ as

$$G(\lambda_i) = 24\eta\left(\frac{\epsilon_0}{kT}\right)\int_1^\infty x g(x) e^{-\overline{\lambda}x}dx, \tag{17}$$

with

$$x = \frac{r}{\sigma}, \quad \overline{\lambda}_i = \lambda_i\sigma^*, \quad \sigma^* = \frac{\sigma}{\sigma_0}, \quad A_Q = \frac{\hbar^2 N_A}{\epsilon_0\sigma_0^2 M_{H_2}} = 0.0835. \tag{18}$$

Detailed expressions for $G(\lambda)$ can be found in a simple form in Refs. [19,20]. Having defined the various parts of the Helmholtz energy F, Eq. (2) can then be readily used to obtain the EOS.

III. LIQUID-VAPOR EQUILIBRIUM OF H_2

The computation of liquid-vapor (L-V) equilibrium is a testing ground of the theoretical formalism as it encounters the transition from a short-range order of the liquid phase to a high-temperature disorder of the vapor phase. The difference between liquid and vapor densities $(\rho_l - \rho_v)$ is zero at the critical temperature $T = T_c$ and nonzero for $T < T_c$. The isotherm has a point of inflection and, therefore, the isothermal compressibility κ_T diverges at $T = T_c$. In the neighborhood of criticality, the implication is that the tendency of separation entails long-range fluctuations and the radial distribution function $g(r)$ must become so long-ranged that $\int [g(r) - 1] d^3\vec{r}$ diverges as $T \to T_c$.

At a given temperature, the coexisting bulk densities of liquid (l) and vapor (v) phases are obtained by solving the simultaneous equations

$$P_l(\rho_l, T) = P_v(\rho_l, T), \tag{19}$$

$$\mu_l(\rho_l, T) = \mu_v(\rho_l, T), \tag{20}$$

where P_i and μ_i $(= F_i + P_i/\rho_i)$ are pressures and chemical potentials for phase i. P_i and F_i have been respectively obtained from Eqs. (1) and (2). The resulting L-V coexistence curves are plotted in Fig. 1. These are compared with the Monte Carlo results [21]. The impact of various corrections (like dimerization and quantum corrections) to the Helmholtz free energy considered here are shown in the phase diagram. The dimerization and quantum energies improve the results to yield closer agreement with the simulation results.

On the other hand, the near vicinity of the critical point can only be treated correctly by the renormalization group methods, which gives a nearly flat curve at this region exactly as the empirical curve. All theoretical models based on the mean approximation give a parabolic coexistence curve in the critical region. Our calculations, based on the inverse temperature expansion of $g(r)$ (see Refs. [17–19]), which is in general a mean field approach, give a parabolic coexistence curve. Remarkably, the quantum correction to the free energy F_Q [Eq. (16)] improves the coexistence curve, even at the near vicinity of the critical point.

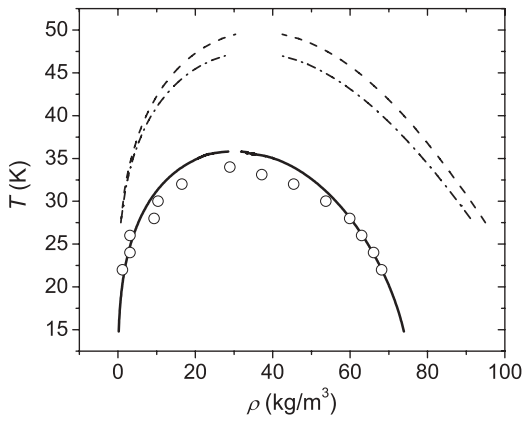

FIG. 1. Liquid-vapor coexistence lines for H_2. Dashed curves are coexistence lines without dimerization [the bond length $L = 0.0$ and the nonsphericity parameter $a = 1.0$, Eqs. (7)–(9)] and without quantum effects, dotted-dashed curves include dimerization effects only (with $L = 0.622$ and $a = 1.154$), solid curves include both dimerization and quantum effects, and open circles are computer simulation results [21].

IV. TEMPERATURE AND PRESSURE DEPENDENCE OF THE COMPRESSIBILITY FACTOR AND DENSITY

The relation for compressibility factor $Z(=\beta p/\rho = \eta \partial \beta F/\partial \eta)$ can be obtained from Eqs. (1) and (2) as

$$Z = 1 + a(Z_{\rm SS} - 1) + Z_{\rm t} + Z_{\rm Q}, \tag{21}$$

with

$$Z_{\rm SS} = \frac{1 + \eta + \eta^2 - a_1\eta^3 - a_2\eta^4}{(1-\eta)^3} - \frac{\eta}{2}[1 + 4\eta + 4\eta^3], \tag{22}$$

$$Z_{\rm t} = \frac{\overline{V} E \eta}{2\sigma^*}[e^{\lambda_1} G'(\bar{\lambda}_1) - e^{\lambda_2} G'(\bar{\lambda}_2)], \tag{23}$$

$$Z_{\rm Q} = \frac{A_Q \overline{V} E \eta}{24\sigma^*}\left(\frac{\epsilon_0}{kT}\right)\left[\lambda_1^2 e^{\lambda_1} G'(\bar{\lambda}_1) - \lambda_2^2 e^{\lambda_2} G(\bar{\lambda}_2)\right], \tag{24}$$

where

$$G' = \left(\frac{\partial G(\bar{\lambda}_i)}{\partial \eta}\right)_T. \tag{25}$$

The first term of Eq. (21), $Z = 1.0$, represents the ideal gas compressibility factor while in the second term, $a(Z_{\rm SS} - 1)$, the nonsphericity parameter a acts on the packing term of the soft sphere compressibility factor, i.e., the excess above the ideal gas value. Largo and Solana [4] considered $a(Z_{\rm HS} - 1)$, but since we are using a softening correction term to the EOS, then $Z_{\rm HS}$ can be replaced by $Z_{\rm SS}$.

The first term of Eq. (22) is the usual hard sphere compressibility factor $Z_{\rm HS}$ given by Baus and Colot [12], with $a_1 = a_2 = \frac{2}{3}$. At low densities Z tends to its ideal value of 1. For example, as $\rho \to 0$, then $Z_{\rm t} \to 0$, $Z_{\rm Q} \to 0$, and $Z^{\rm HS} \to 1$.

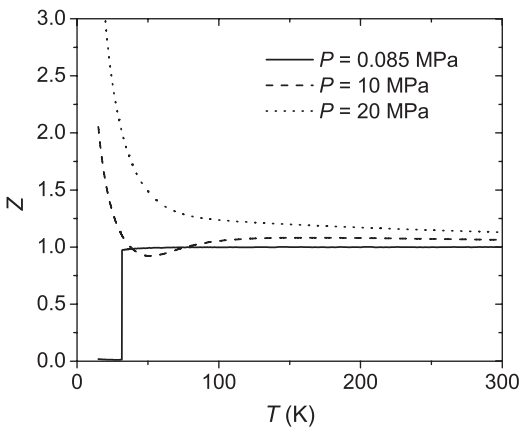

FIG. 2. Compression factor for H_2 as a function of temperature at different pressures.

On the other hand, at very high densities, Z increases sharply with decreasing T. $Z > 1$ indicates that repulsive forces are dominant in the system, whereas $Z < 1$ can be related to the dominance of the attractive forces.

The computed values of Z as function of T are plotted n Fig. 2 for $P = 0.85$, 10.0, and 20.0 MPa. At $T \geqslant 150$ K, Z becomes flat towards its ideal value and the impact of T and P is quite small. However, the impact of pressure and temperature on Z is quite significant for $T < 100$ K. In the range of pressure 20.0 MPa, Z increases sharply as T decreases. At lower pressures, say at 0.85 MPa, Z decreases with temperature and has values significantly lower than the ideal value.

The computed values of the density of H_2 as a function of T for different pressures $p = 0.85$, 10, and 20 MPa are plotted in Fig. 3. These are compared with the available computer simulation results [21]. The agreement of the computed values with simulation results is very much encouraging. The impact of the quantum correction term [Eq. (24)] is very much evident in the low-temperature range. At $p = 0.85$ MPa [Fig. 3(a)], the quantum correction becomes effective at $T \leqslant 40$ K, shifting to $T \leqslant 140$ K at $p = 10$ MPa [Fig. 3(b)] and $T \leqslant 200$ K at $p = 20$ MPa [Fig. 3(c)]. The steep fall of the density is quite dramatic in the low-temperature region at $p = 0.85$ MPa. As expected, the density increases with increasing pressure at any given temperature.

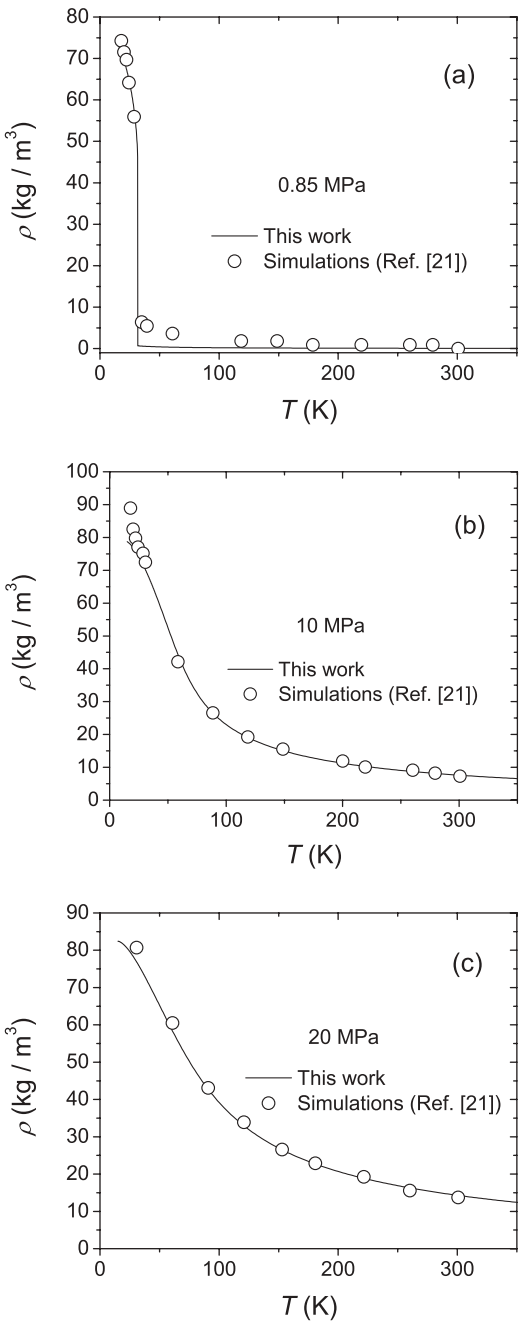

FIG. 3. Comparison of the variation of H_2 density with temperature at (a) $p = 0.85$ MPa, (b) $p = 10$ MPa, and (c) $p = 20$ MPa. Here, the solid curves are results of this work and open circles are computer simulations [21].

V. THERMOPHYSICAL PROPERTIES

A. Entropy and specific heat

The formalism of Sec. II allows us to compute the temperature dependence of the Helmholtz free energy, which, in turn, yields entropy (S) and the specific heats (C_P and C_V). With the Gibbs free energy $G = F + P/\rho$, we have,

$$S = -\left(\frac{\partial G}{\partial T}\right)_P = -\left[\frac{\partial (F_{\rm id} + F_{\rm HCB} + F_{\rm t} + F_{\rm Q})}{\partial T}\right]_P + \frac{P}{\rho^2}\left(\frac{\partial \rho}{\partial T}\right)_P, \quad (26)$$

$$C_P = T\left(\frac{\partial S}{\partial T}\right)_P = -T\left(\frac{\partial^2 G}{\partial T^2}\right)_P, \quad (27)$$

$$C_V = T\left(\frac{\partial S}{\partial T}\right)_\rho = -T\left(\frac{\partial^2 F}{\partial T^2}\right)_V. \quad (28)$$

It may be noted that F's and P's are functions of σ, which in our scheme is T dependent [see Eq. (14)]. Hence, F's and P's contribute to entropy and specific heat.

The effect of temperature and pressure on the excess entropy, relative to the ideal gas entropy $S_{\rm id}$, $S_{\rm xs}$ ($= S - S_{\rm id}$) is shown in Fig. 4. $S_{\rm xs}$ provides a quantitative measure of the system structural ordering. It may be viewed as an effective

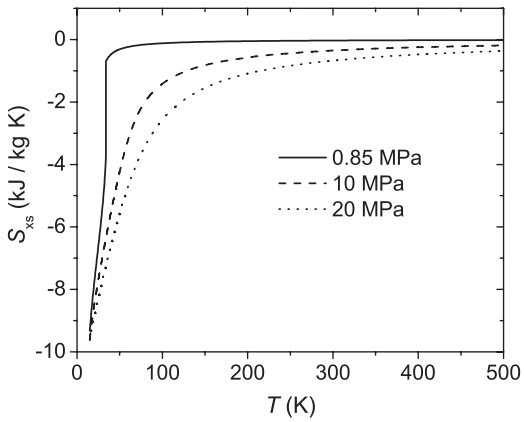

FIG. 4. Variation of excess entropy $S_{\rm xs}$ with temperature at different pressures.

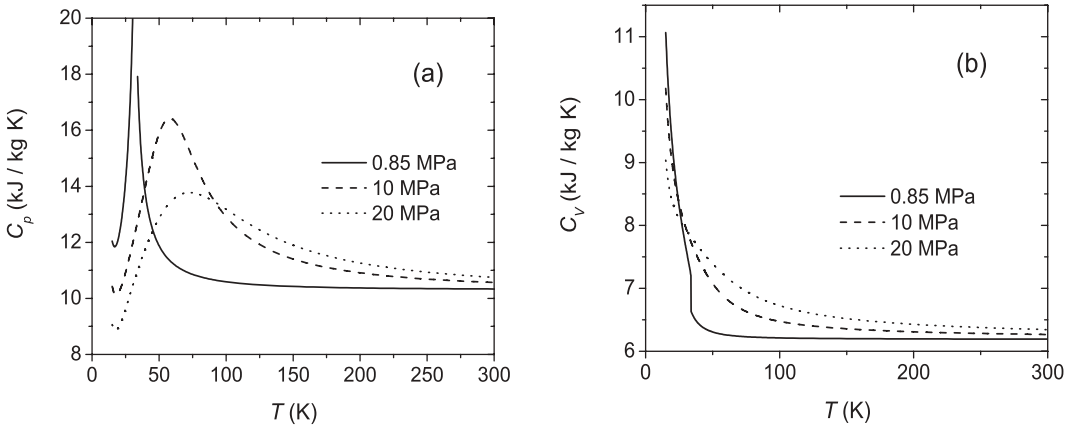

FIG. 5. Plots of (a) C_P and (b) C_V for H_2 as functions of temperature at different pressures.

thermodynamic function to assess stability, particularly at extreme T and p. It is often argued that S_{xs} is a better thermodynamic function to map the ordering in the system than the structure factor. S_{xs} for H_2 is found to be quite sensitive at low temperatures and at high pressures. S_{xs} falls rapidly with $T \leqslant 100$ K at higher pressures. At higher temperatures it tends to zero, i.e., towards ideal entropy. As expected, S_{xs} decreases with increasing p at any given temperature.

Computed values of C_P and C_V as functions of temperature for different pressures $P = 0.85$, 10, and 20 MPa are plotted in Fig. 5. C_P [Fig. 5(a)] exhibits anomalous behavior at these pressures for lower temperatures, $T \leqslant 100$ K. C_P increases with T, showing a maximum, and then starts decreasing. The maxima get sharpened at low pressure, $P = 0.85$ MPa. Such a characteristic behavior of C_P has also been observed in undercooled [22–24] liquid metals. The inflection in C_P might be a signature of the configurational transformation and possibly could be viewed as structural freezing, which is dictated by P and T. The temperature at which C_P is maximum in undercooled liquid metals is often interpreted [25] as glass transition temperature. Contrary to C_P, C_V [Fig. 5(b)] does not exhibit a similar behavior. C_V is found to increase sharply in the low-temperature region.

One of the sensitive quantities that tests the limitations of the formalism presented in this work is specific heat ration $\gamma = (C_P/C_V)$, which plays a vital role in thermophysical characterization. It appears in many fluid equations during a simple compression and expansion process, the equation of speed of sound, and all equations of isentropic flows and shock waves. The computed values of γ for different P and T are plotted in Fig. 6. As expected, γ fluctuates considerably in the low-temperature range due to anomalies in C_P. At high temperature, γ remains invariant and tends to a constant value $\gamma = 1.67$. It may be noted that for an ideal gas model, γ varies from 1.33 (polyatomic system) to 1.67 (monatomic system). Our formalism, however, gives $\gamma = 1.67$ in the ideal gas conditions. The reason for this is that when treating for H_2 dimerization, the H_2 molecule is replaced by an effective spherical, monatomic particle.

The thermodynamic definition of the adiabatic parameter is $\gamma = (\chi_T/\chi_S)$, the ratio of isothermal to adiabatic compressibilities. Therefore, the dramatic fluctuations of γ at low temperatures may also be attributed to the divergence of the isothermal compressibility in approaching the phase transition region.

B. Isothermal compressibility and thermal expansion

The computed values of the temperature and pressure dependent density (see Sec. III) allow us to evaluate the

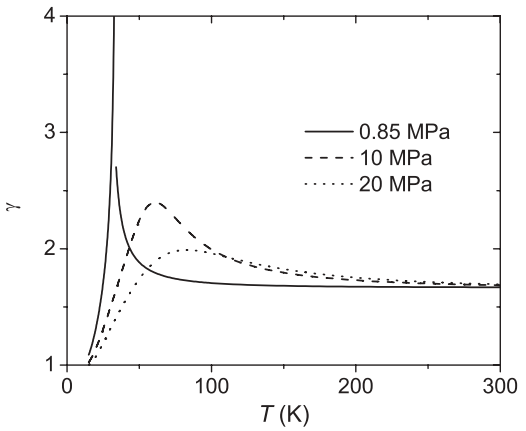

FIG. 6. The ratio $\gamma = C_P/C_V$ vs temperature at different pressures.

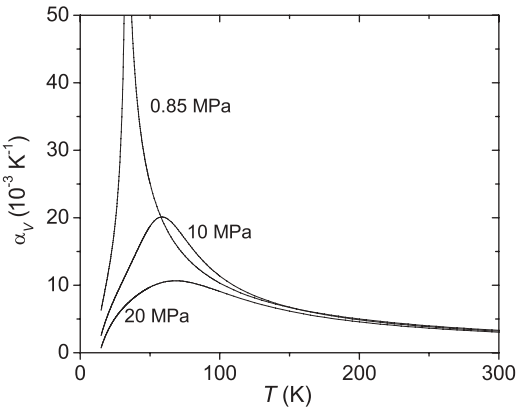

FIG. 7. The coefficient of volume expansion α_V vs temperature at different pressures.

coefficient of volume expansion (α_V) and the isothermal compressibility (χ_T):

$$\alpha_V = -\frac{1}{\rho}\left(\frac{\partial \rho}{\partial T}\right)_P, \tag{29}$$

$$\chi_T = \frac{1}{\rho}\left(\frac{\partial \rho}{\partial P}\right)_T. \tag{30}$$

α_V and χ_T are important thermophysical functions for dense fluids which evaluate its expansion and contractions under various conditions of temperature and pressure. Most of the systems exhibit positive α_V, except liquid water between 0°C and 4°C, where the expansion coefficient is negative. Many other substances [26] are also found to show negative expansion coefficients. The computed values of α_V for H_2 as a function of T (<400 K) and P (0.85, 10.0, and 20.0 MPa) are shown in Fig. 7. The impact of T and P on α_V in the lower temperature range ($T < 150$ K) is very dramatic. α_V increases sharply as temperature decreases below 150 K. α_V tends to get maximum and then decreases. The maxima are sharper at lower pressures, say, at 0.85 MPa, and become flatter at higher pressures. However, at high temperatures, the effect of pressure on α_V is found to be minimal: α_V varies little at high T and P.

The computed values of isothermal compressibility χ_T are plotted in Fig. 8(a) versus temperature for different pressures. At lower pressure $P = 0.85$ MPa and lower temperature $T \approx 50$ K, χ_T is quite different than its value at other pressures and temperatures. At temperatures $\geqslant 100$ K, χ_T remains almost constant.

Isentropic compressibility $\chi_S (= \chi_T/\gamma)$ has been computed using our values of χ_T and γ. These are plotted for different P and T in Fig. 8(b). χ_T at $P = 0.85$ MPa is quite high compared to χ_S at 10 and 20 MPa. Unlike χ_T, χ_S does not exhibit a sharp peak in the lower range of temperature.

VI. VELOCITY OF SOUND

Isentropic compressibility χ_S and the density can readily be used to determine the velocity of sound in H_2 as a function of P and T,

$$v_l(T,P) = [\rho(P,T)\chi_S(P,T)]^{-1/2}. \tag{31}$$

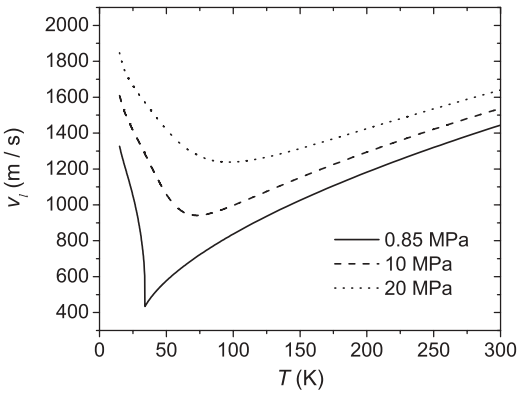

FIG. 9. The velocity of sound v_l in H_2 vs temperature at different pressures.

The velocity of sound is of high importance as it is related to different thermodynamic properties, such as surface tension and dynamics of interfaces [27,28], heat capacity [29], boiling and critical points [30], and the Gruneisen parameter [31]. Sound velocity for different substances and mixtures has also been extensively tabulated [32].

The computed values of v_l are plotted in Fig. 9. At a given temperature, v_l increases with increasing pressure. At high P and T, v_l increases almost linearly with increasing temperature. v_l changes drastically with P and T in the range of temperature $\leqslant 100$ K. It exhibits a minimum at a given pressures and temperature.

VII. SUMMARY AND CONCLUSION

A realistic equation of state for H_2 forms the basis to investigate the phase stability, thermodynamic properties, and connection to other thermophysical properties. The present formalism includes the long-range attractive interaction among the constituent species via the double Yukawa (DY) potential, which acts as a perturbation on the reference hard sphere system. The advantage of using the DY potentials is that it allows the variational integral equations of the energies to be determined analytically in terms of the Laplace transform of the radial distribution function. The dimerization of the H_2 molecules is treated as a hard convex body fluid, and the quantum effect, which is necessary for a light-particle system,

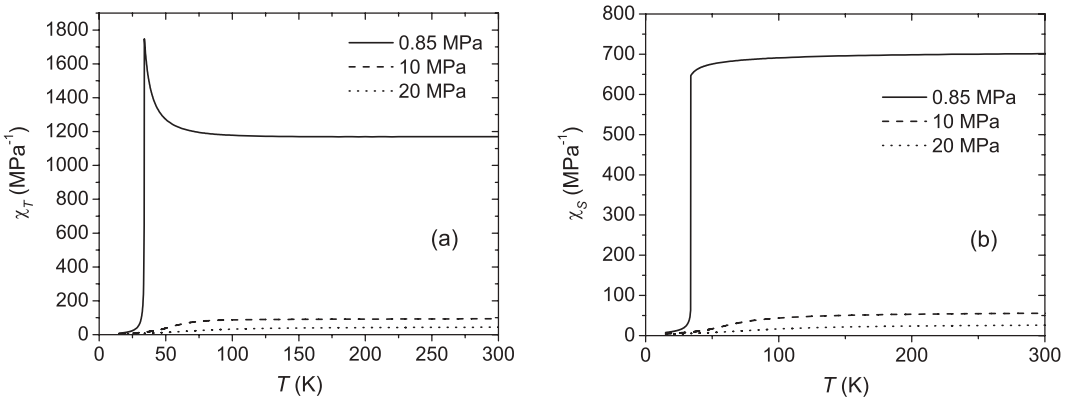

FIG. 8. Plots of (a) isothermal compressibility χ_T and (b) isentropic compressibility χ_S vs temperature at different pressures.

is included via the first-order quantum correction to the free energy in the Wigner-Kirkwood expression.

We utilized our formalism to compute the liquid-vapor coexistence curve. The values are in good agreement with the Monte Carlo simulation results. The results suggest that the correction for dimerization and, especially, the quantum effect to the Helmholtz free energy are very important. The computed values of densities as functions of temperature for different pressures are also found to be in good agreement with computer simulation results. Again, the quantum correction to the Helmholtz free energy is essential, particularly, in the low-temperature region.

The impact of pressure and temperature on C_P is distinctly visible in the low-temperature region: C_P rises anomalously for $T \leqslant 100$ K and exhibits maxima at a given temperature. This is interpreted as a signature of configurational transformation with structural freezing. Contrary to C_P, the velocity of sound is found to exhibit minima at certain temperatures below 100 K. The compressibility increases with decreasing pressure and remains almost invariant for $T \geqslant 100$ K.

The present formalism can be utilized to investigate the thermodynamic properties of H_2 near the liquid-vapor coexistence curve, which we intend to pursue in a later work.

[1] S. T. Weir, A. C. Mitchell, and W. J. Nellis, Phys. Rev. Lett. **76**, 1860 (1996).
[2] W. J. Nellis, Space Sciences **48**, 671 (2000).
[3] M. J. Maeso and J. R. Solana, J. Chem. Phys. **100**, 3142 (1994); **101**, 9864 (1994); **104**, 4728 (1996); Mol. Phys. **99**, 371 (2001).
[4] J. Largo and J. R. Solana, Phys. Rev. E **58**, 2251 (1998); Mol. Phys. **96**, 1367 (1999).
[5] E. P. Wigner, Phys. Rev. **40**, 749 (1932).
[6] J. G. Kirkwood, Phys. Rev. **44**, 749 (1933).
[7] H. F. Ree and C. F. Bender, J. Chem. Phys. **71**, 53621 (1979).
[8] J. Grafenstein and D. Cremer, Mol. Phys. **99**, 981 (2001).
[9] V. M. Rozenbaum, A. M. Mebel, and S. H. Lin, Mol. Phys. **99**, 1883 (2001).
[10] D. T. Chang, G. Surrat, G. Ristroff, and G. I. Gellene, J. Chem. Phys. **116**, 9188 (2002).
[11] N. C. Handy, Mol. Phys. **100**, 77 (2002).
[12] M. Baus and J. L. Colot, Phys. Rev. A **36**, 3912 (1987).
[13] M. Ross, J. Chem. Phys. **71**, 1567 (1979).
[14] I. F. Silvera and V. V. Goldman, J. Chem. Phys. **69**, 4209 (1978).
[15] H. Jones, J. Chem. Phys. **55**, 2640 (1971).
[16] S. M. Osman and W. H. Young, Phys. Chem. Liq. **17**, 181 (1987).
[17] D. Henderson, L. Blum, and J. P. Noworyta, J. Chem. Phys. **102**, 4973 (1995).
[18] D. Henderson, L. Mier-y-Teran, and L. Blum, Fluid Phase Equilib. **130**, 65 (1997).
[19] D.-M. Duh and L. Mier-y-Teran, Mol. Phys. **90**, 373 (1997).
[20] M. Bahaa Khedr, S. M. Osman, and M. S. Al Busaidi, Mol. Phys. **107**, 1355 (2009).
[21] Q. Wang, J. K. Johnson, and J. Q. Broughton, Mol. Phys. **89**, 1105 (1996).
[22] T. Shen and J. T. Wang, J. Non-Cryst. Solids **117-118**, 559 (1990).
[23] J. J. Perepezko and J. S. Paik, J. Non-Cryst. Solids **61-62**, 113 (1984).
[24] R. N. Singh and F. Sommer, Phys. Chem. Liq. **28**, 129 (1994).
[25] R. N. Singh and R. P. Jaju, Physica B **240**, 133 (1997).
[26] G. D. Barrera, J. A. O. Bruno, T. H. K. Barron, and N. L. Allan, J. Phys: Condensed Matter **17**, R217 (2005).
[27] S. Blairs, J. Colloid. Interf. Sci. **302**, 312 (2006).
[28] S. Magazu and G. Maisano, J. Mol. Liq. **93**, 7 (2001).
[29] K. A. Gillis, I. I. Shinder, and M. R. Moldover, Phys. Rev. E **70**, 021201 (2004).
[30] R. T. Lagemann and W. S. Dunbar, J. Phys. Chem. **49**, 428 (1945).
[31] R. K. Shukla, S. K. Shukla, V. K. Pandey, and P. Awasthi, Phys. Chem. Liq. **45**, 169 (2007).
[32] H. N. V. Temperley and J. S. Rowlinson, *Physics of Simple Liquids* (North Holland, Amsterdam, 1968).